An Efficient Analytic Approach for Calculation of Multi-Dimensional Franck-Condon Factors and Associated Photoelectron Spectra.

Tosaporn Sattasathuchana,[a] Riccardo Murri,[b] and Kim K. Baldridge[a,c]*

[a]Department of Chemistry, University of Zurich, Winterthurerstrasse 190, CH-8057 Zurich, Switzerland

[b]Service and Support for Science IT, University of Zurich, Winterthurerstrasse 190, CH-8057 Zurich, Switzerland

[c]Health Science Platform, Tianjin University, 92 Weijin Road, Nankai District, Tianjin, 300072, China

Supplementary Information

I. THEORETICAL METHODS

I.1. *Ab initio* Quantum Chemical and Density Functional Theory Methods

The optimization and vibrational analysis of both initial and final states needed to evaluate FC integrals and associated PES were carried out using the GAMESS software.[1] The levels of theory used for each of the applications were selected based on a performance analysis to provide optimal accuracy for the electronic structure, vibrational frequencies and simulated photoelectron spectra. For the 3-D FC application of H_2O and H_2O^+ cation $\widetilde{B}^2B_2$ state, the completely renormalized Coupled-Cluster method (CR-CC(2,3))[2,3] together with aug-cc-pVTZ basis set was used. For both the 15-D case of syn and anti vinyl alcohol and 30-D case of benzene cation, DFT was employed using the ωB97x-D functional[4] together with the Def2-TZVPPD basis set.[5] The choice of this functional was based on a comparative analysis across a broad array of functionals and conventional wavefunction theory. Full geometry optimizations were performed and uniquely characterized via second derivative (Hessian) analysis to determine stationary states as well as to obtain vibrational frequencies and normal mode data for FC computations. In all DFT calculations, an army grade grid was used for radial points in the Euler-MacLaurin quadrature and Lebedev grids (NRAD=155 and NLEB=1202, respectively).

I.2. Deconvolution of Spectra

The representation of spectra is dependent on the spectral bandwidth and resolution and not on the methodology used to deconvolute the spectra. The spectral bands are typically fit to either Gaussian or Lorentzian functions.[6] The Gaussian function is more applicable to UV-Vis spectra, while the Lorentzian function is more applicable to NMR spectra.[6] Online resources are available for generation of photoelectron/photodetachment spectra for polyatomic molecules, such as eZspectrum,[7] where Franck-Condon factors (FCF) are calculated as overlaps of 1-D harmonic

wave functions and neglecting mode mixing.[7] In the present work, a spectrum generating program has been created using Gaussian functions for the general case of multi-dimensional FCFs, including Duschinsky rotation (mode mixing).

A peak of the Gaussian line shape is governed by the function

$$I = A \exp\left[-(4\ln 2)\left(\frac{\nu - \nu_{max}}{\Delta\nu}\right)^2\right] \qquad \text{(s1)}$$

where I is the intensity of the peak, A is the oscillator strength (FCF value), ν_{max} is the energy at the band maximum, ν is an arbitrary energy, and $\Delta\nu$ is the full width at half maximum (FWHM) value. The resolution of the spectra is dependent on the FWHM, for example, higher values of FWHM correspond to a broadening of the peak. The complete spectrum is the sum of the individual Gaussian bands as,

$$I = \sum_i A_i \exp\left[-(4\ln 2)\left(\frac{\nu - \nu_{i,max}}{\Delta\nu_i}\right)^2\right] \qquad \text{(s2)}$$

I.3. Handedness of Coordinate system

The Cartesian coordinate system has two orientations as determined by the handedness. Defining the xy-plane as the plane of the paper and the z-axis to be coming out of that plane, the representation is "right-handed" (e.g., Figure S1a). If the direction of the z-axis is into the plane (e.g., Figure S1b), the representation is "left-handed." When the xy-plane of the left and the right handed representations are overlayed, the z-axes of the left and right handed representations will 180° opposed.

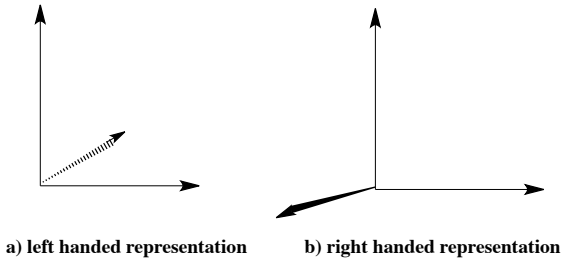

Figure S1. Cartesian coordinate representations for a) left handed and b) right handed coordinate systems.

I.3.1. Rotational matrix

With reference to the coordinate axis, there are three possibilities for rotation: rotation about the x-axis or *Pitch*,[8] rotation about the y-axis, or *Heading*,[8] and rotation about the z-axis, or *Bank*.[8] These are briefly defined as follows.

I.3.1.1 Pitch: The positive rotation about the x-axis in the left-handed coordinate system is clockwise. After the pitch rotation, the yz-plane is rotated by θ_l. In Figure S2a, the new $+Y_l$ and $+Z_l$ represent the coordinate axis change due to the rotation (black to red). The pitch matrix is

$$P_l = \begin{bmatrix} 1 & 0 & 0 \\ 0 & \cos(\theta_l) & -\sin(\theta_l) \\ 0 & \sin(\theta_l) & \cos(\theta_l) \end{bmatrix}$$

In contrast, the positive rotation about the x-axis in the right-handed coordinate system is counterclockwise. After the pitch rotation, the yz-plane is rotated by θ_r. The new $+Y_l$ and $+Z_l$ axes are depicted in red in Figure S2b. The pitch matrix in this case is

$$P_r = \begin{bmatrix} 1 & 0 & 0 \\ 0 & \cos(\theta_r) & -\sin(\theta_r) \\ 0 & \sin(\theta_r) & \cos(\theta_r) \end{bmatrix}$$

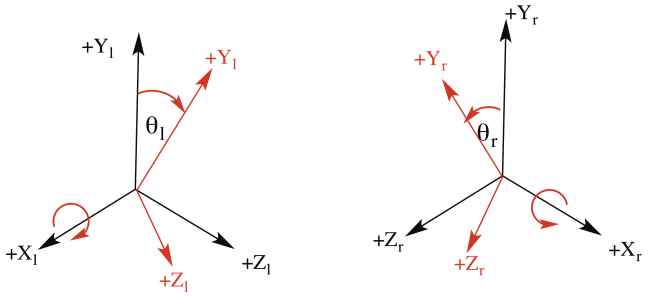

a) left handedness b) right handedness

Figure S2. (a) Rotation about the x-axis in the left-handed coordinate system, and (b) Rotation about the x-axis in the right-handed coordinate system.

I.3.1.2 Heading: Rotations about the y-axis for both left-handed and right-handed coordinate systems are illustrated in Figure S3. The clockwise rotation about the $+Y_l$-axis results in the change of $+X_l$ and $+Z_l$ axis, as represented by the red axis. The rotational matrix of Heading is

$$H_l = \begin{bmatrix} \cos(\theta_l) & 0 & \sin(\theta_l) \\ 0 & 1 & 0 \\ -\sin(\theta_l) & 0 & \cos(\theta_l) \end{bmatrix}$$

The rotation in the right-handed coordinate system is counterclockwise. The positive angle of this rotation is θ_r, and the heading matrix is

$$H_r = \begin{bmatrix} \cos(\theta_r) & 0 & \sin(\theta_r) \\ 0 & 1 & 0 \\ -\sin(\theta_r) & 0 & \cos(\theta_r) \end{bmatrix}$$

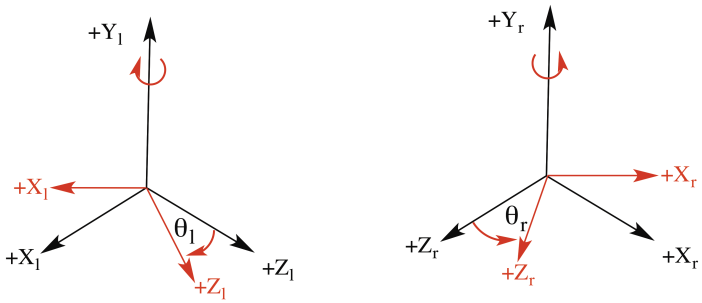

a) left handedness b) right handedness

Figure S3. Representation of rotation about the y-axis in the (a) left-handed and (b) right-handed coordinate systems.

I.3.1.3 Bank: A positive rotation about the $+Z_l$-axis is clockwise. The bank angle is θ_l, as depicted in Figure S4a. The bank matrix is,

$$B_l = \begin{bmatrix} \cos(\theta_l) & -\sin(\theta_l) & 0 \\ \sin(\theta_l) & \cos(\theta_l) & 0 \\ 0 & 0 & 1 \end{bmatrix}$$

Positive rotation about the $+Z_r$-axis is counterclockwise (Figure S4b). As a result, the bank matrix in the right-handed coordinate system is given as

$$B_r = \begin{bmatrix} \cos(\theta_r) & -\sin(\theta_r) & 0 \\ \sin(\theta_r) & \cos(\theta_r) & 0 \\ 0 & 0 & 1 \end{bmatrix}$$

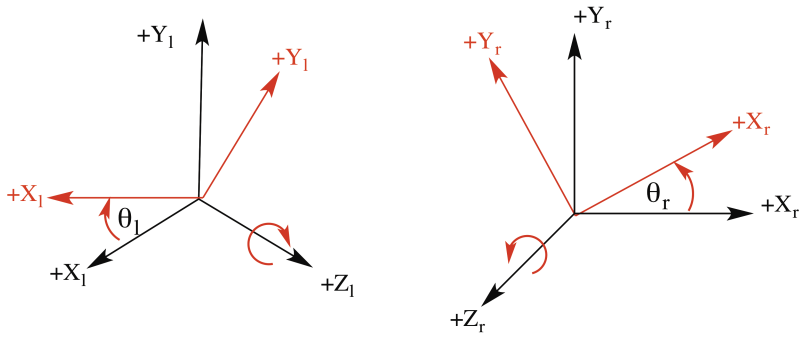

a) left handedness b) right handedness

Figure S4. Rotation about the z-axis in the (a) left-handed and (b) right-handed coordinate systems.

The rotational matrices for operation on x-, y-, and z- axes are composed of heading, pitch, and bank matrices. The left-handed rotation is determined as,

$$R_l = H_l P_l B_l \qquad \text{(s3)}$$

and the rotation in the right-handed coordinate system as determined from the left-handed system is

$$R_r = S_z R_l S_z \qquad \text{(s4)}$$

where

$$S_z = \begin{bmatrix} 1 & 0 & 0 \\ 0 & 1 & 0 \\ 0 & 0 & -1 \end{bmatrix}$$

The right-handed and left-handed systems are related by $Q_r=S_zQ_l$. Using the rotational relationship in Eqn S5, the transformation of the right-handed coordinate system is given by

$$Q'_r = S_z Q'_l = S_z R_l Q_l = S_z R_l S_z Q_r \quad \text{(s5)}$$

For correct determination of FCF and associated photoelectron spectra, the coordinate system must be consistent from the ground to the excited states. There is a noticeable effect of handedness on the results of the FC calculation and associated prediction of photoelectron spectra.

II. 1-D FCF Mathematical Formalism

Vibronic transitions are governed by the Franck-Condon principle, such that the probability of transition involves the overlap integral of the initial state and final state, e.g., Franck-Condon Factor (FCF).[9,10] The transition probability (P) is given as,

$$P = |\langle \psi_g | \psi_f \rangle|^2 \quad \text{(s6)}$$

where ψ_g and ψ_f are the electronic vibrational of wavefunction of the ground and the excited states, respectively.

Under the assumption of the harmonic oscillator approximation, the 1-D vibronic wavefunctions is,

$$|\upsilon\rangle = N_\upsilon H_\upsilon(\sqrt{\alpha}x) \exp\left(-\frac{1}{2}\alpha x^2\right) \quad \text{(s7)}$$

where N_υ is a normalized factor, $N_\upsilon = \left(\frac{\sqrt{\alpha}}{2^\upsilon \upsilon!\sqrt{\pi}}\right)^{1/2}$, $H_\upsilon(x)$ is the Hermite polynomial, and α is a function of the frequency, $\alpha = \frac{\omega}{\hbar}$ with angular frequency, ω, and $\hbar$ Planck's constant.

The ground state geometry is typically altered during the excitation process as manifested by displacement and/or distortions of the involved normal modes. In this case, the overlap integral between the two vibrational states is,

$$\langle \upsilon | \upsilon' \rangle = N_\upsilon N_{\upsilon'} \int_{-\infty}^{\infty} H_\upsilon\left(\sqrt{\alpha}x\right) H_{\upsilon'}\left(\sqrt{\alpha'}x'\right) \times \exp\left(-\frac{1}{2}\alpha x^2 - \frac{1}{2}\alpha' x'^2\right) dx \quad \text{(s8)}$$

where the prime and non-primed values refer to the initial and final states, respectively. The displacement (d) between the equilibrium ground (x') and excited (x) states can be determined from

$$x' = x + d \quad \text{(s9)}$$

Using Eqn s9 and substituted to Eqn s8, one obtains[11]

$$\langle \upsilon | \upsilon' \rangle = N_\upsilon N_{\upsilon'} \exp\left(-\frac{S}{2}\right) \int_{-\infty}^{\infty} H_\upsilon\left(\sqrt{\alpha x}\right) H_{\upsilon'}\left(\sqrt{\alpha' x'} + \sqrt{\alpha' d}\right) \times \exp\left(-\frac{\alpha + \alpha'}{2}\left(x + \frac{\alpha' d}{\alpha + \alpha'}\right)^2\right) dx \quad \text{(s10)}$$

where $S = \frac{\alpha \alpha' d^2}{\alpha + \alpha'}$. Substituting $y = x + \frac{\alpha' d}{\alpha + \alpha'}$ into Eqn s10,

$$\langle \upsilon | \upsilon' \rangle = N_\upsilon N_{\upsilon'} \exp\left(-\frac{S}{2}\right) \int_{-\infty}^{\infty} H_\upsilon\left(\sqrt{\alpha}y + b\right) H_{\upsilon'}\left(\sqrt{\alpha'}y + b'\right) \times \exp\left(-\frac{\alpha + \alpha'}{2} y^2\right) dy \quad \text{(s11)}$$

where $b = -\frac{\alpha'\sqrt{\alpha}d}{\alpha+\alpha'}$ and $b = -\frac{\alpha\sqrt{\alpha'}d}{\alpha+\alpha'}$. Using the properties of Hermite polynomials in Eqn s12,

$$H_n(x+d) = \sum_{k=0}^{n} \binom{n}{k} H_{n-k}(d)(2x)^k \tag{s12}$$

and the well-known Gaussian integral in Eqn s13, which is nonzero when k + k' is even,

$$\int_{-\infty}^{\infty} x^{2n} \exp(-ax^2)dx = \frac{(2n-1)!!}{(2a)^n}\left(-\frac{\pi}{\alpha}\right)^{1/2} \tag{s13}$$

where $(2n-1)!! = 1\times3\times5\times\ldots\times(2n-1)$, the overlap integral in Eqn s11 becomes

$$\langle v|v'\rangle = \left(\frac{Ae^{-S}}{2^{v+v'}v!v'!}\right)^{1/2} \sum_{k=0}^{v}\sum_{k'=0}^{v'} \binom{v}{k}\binom{v'}{k'} H_{v-k}(b)H_{v'-k'}(b') \times \left(2\sqrt{\alpha}\right)^k \left(2\sqrt{\alpha'}\right)^{k'} I(K) \tag{s14}$$

where $A = \frac{2\sqrt{\alpha+\alpha'}}{\alpha+\alpha'}$, and

$$I(K) = \begin{cases} 0 & \text{, k+k' is odd} \\ \frac{(2K-1)!!}{(\alpha+\alpha')^K} & \text{, k+k' is even} \end{cases} \tag{s15}$$

with $K = (k+k')/2$.

The Franck Condon Integral (FCI) can be determined completely from Eqn s14.[11] This 1-D FCI can be applied to diatomic molecules (e.g., one normal mode).

III. Supplementary Figure of the photoelectron spectra of H_2O^+ ($\widetilde{B}^2B_2$) demonstrating the influence of handedness assignment.

In this particular case, the handedness of the asymmetric stretching mode does not appear to affect the intensity of the PES, as illustrated by comparison of Figure S5c (l, l, r) with Figure S5e

(l, l, l), which shows that the spectral bands are identical. This is due to the fact that the corresponding Duschinsky matrices have zero values for J_{13}, and J_{23}, an indication of no coupling to this normal mode. A 'l' and 'r' triplet notation has been introduced to show the effects of the handedness on the prediction of the spectra. Figure S5b, Figure S5c and Figure S5d with mode assignments (r, r, r), (l, l, r) and (l, l, l), with the remaining two normal modes (symmetric stretch and bend) having the same handedness, result in essentially identical PES results, however with the resulting intensity higher and information about the progression of transitions more than when the spectra are determined using a mixture of handedness, such as (l, r, x). All three of these last spectra provide similar spectral band shapes as determined by Chang (Figure S5f).

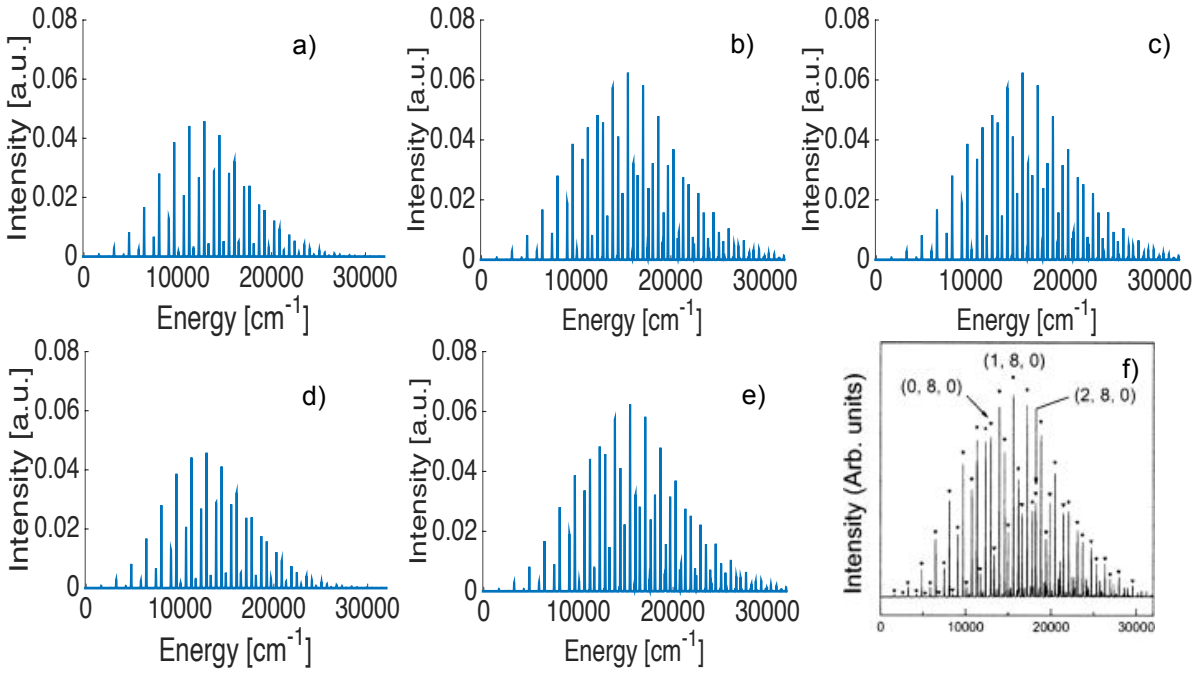

Figure S5. Simulated photoelectron spectra of H_2O^+ ($\tilde{B}^2B_2$) with FWHM 50 cm^{-1} calculated at CR-CC(2,3)/aug-cc-pVTZ level of theory for coordinate assignments as a) (l,r,r) b) (r,r,r) c) (l,l,r) d) (l,r,l) e) (l,l,l) f) (U)CCSD(T)/6-311++G(3df,2pd)[12]

IV. Supplementary Table for ground and cation of vinyl alcohol

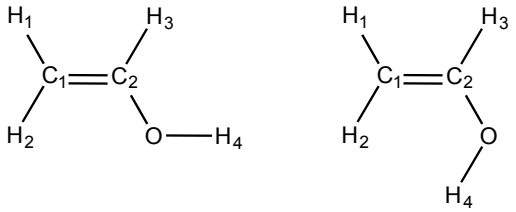

Figure S6. Numbering systems of anti- and syn-vinyl alcohol.

Table S1. ωB97x-D/Def2-TZVPPD optimized geometries of anti- and syn- vinyl alcohol and the respective cation states (reference geometry specifications depicted in Figure S6).

Parameter	Anti-rotamer			Syn-rotamer		
	Neutral		Cation	Neutral		Cation
	Calc.	Expt.[13]	(calc.)	Calc.	Expt.[14]	(calc.)
$O\text{-}H_4$	0.955	0.955	0.955	0.959	0.960	0.971
$C_2\text{-}O$	1.358	1.358	1.358	1.352	1.372	1.275
$C_1\text{-}C_2$	1.322	1.322	1.322	1.325	1.326	1.407
$C_2\text{-}H_3$	1.085	1.085	1.085	1.082	1.097	1.086
$C_1\text{-}H_1$	1.079	1.079	1.079	1.079	1.079	1.082
$C_1\text{-}H_2$	1.081	1.081	1.081	1.083	1.086	1.084
$\angle H_4OC_2$	110.1	110.1	110.1	109.7	126.2	115.7
$\angle OC_2C_1$	122.5	122.5	122.5	126.8	108.3	124.6
$\angle C_1C_2H_3$	121.8	121.8	121.8	122.4	129.1	121.8
$\angle C_2C_1H_1$	119.5	119.5	119.5	119.8	119.5	119.3
$\angle C_2C_1H_2$	121.5	121.5	121.5	122.2	121.7	121.6

Table S2. ωB97x-D/Def2-TZVPPD calculated harmonic vibrational frequencies for anti- and syn- vinyl alcohol and their respective cation states.

Freq.	Anti-rotamer		Syn-rotamer		
	Neutral	Cation	Neutral		Cation
			Calc.	Expt. [15]	
ν_1	3950.5	3757.8	3889.3	3633.5	3731.7
ν_2	3280.5	3292.1	3269.4	3121.7	3280.7
ν_3	3185.1	3165.6	3211.7	-	3203.0
ν_4	3164.4	3178.9	3163.9	-	3157.3
ν_5	1754.7	1644.1	1727.7	1644.5	1623.0
ν_6	1445.7	1483.4	1456.5	1411.8	1492.8
ν_7	1360.9	1325.2	1363.0	1300.0	1429.6
ν_8	1302.2	1391.3	1339.6	1259.7	1308.7
ν_9	1162.6	1159.1	1140.2	1097.9	1154.9
ν_{10}	973.8	1009.8	974.4	947.6	996.3
ν_{11}	491.3	494.4	503.8	-	499.9
ν_{12}	991.2	1040.5	1014.9	972.5	1055.7
ν_{13}	878.3	942.6	852.3	816.7	934.1
ν_{14}	725.6	437.7	723.9	698.9	398.1
ν_{15}	292.1	672.2	456.1	-	694.3

V. Supplementary Table for ground and cation $\widetilde{X}^2E_{1g}$ states of benzene

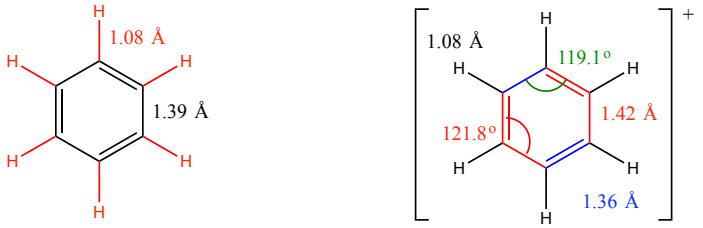

Figure S7. ωB97x-D/Def2-TZVPPD optimized geometry parameters for benzene ground (left) and cation $\widetilde{X}^2E_{1g}$ (right) states.

Table S3. ωB97x-D/Def2-TZVPPD calculated harmonic vibrational frequencies of the ground and cation $\widetilde{X}^2E_{1g}$ state of benzene.

	Symmetry	C_6H_6		$C_6H_6^+(\widetilde{X}^2E_{1g})$	
Mode	(D_{6h})	Calc.	Expt.[16]	Calc.	Expt.[17]
1	A_{1G}	3220.05	3073.94	3242.57	2960.12
2	A_{1G}	1029.72	993.07	994.96	984.02
3	A_{2G}	1390.74	1350.00	1399.69	
4	A_{2U}	697.21		689.62	
5	B_{1U}	3184.33		3210.69	
6	B_{1U}	1033.13	990.00	1021.95	
7	B_{2G}	1040.47	707.00	1046.31	
8	B_{2G}	729.18	1010.00	386.49	
9	B_{2U}	1341.34	1309.40	1416.20	
10	B_{2U}	1178.95	1149.70	1212.19	
11	E_{1G}	881.64	848.90	811.57	
12	E_{1G}	881.64		917.63	
13	E_{1U}	3209.91	3057.70	3239.75	
14	E_{1U}	3209.91		3230.82	
15	E_{1U}	1529.61	1483.99	1462.75	
16	E_{1U}	1529.61		1566.72	
17	E_{1U}	1073.79	1038.27	965.81	
18	E_{1U}	1073.79		1083.00	
19	E_{2G}	3194.09	3047.91	3214.45	
20	E_{2G}	3194.09		3228.11	
21	E_{2G}	1670.21	1609.52	1393.24	
22	E_{2G}	1670.21		1705.94	1588.95
23	E_{2G}	1208.92	1177.78	992.25	
24	E_{2G}	1208.92		1228.95	1290.52
25	E_{2G}	626.62	608.13	325.96	
26	E_{2G}	626.62		605.61	685.59
27	E_{2U}	1014.05	967.00	1044.34	
28	E_{2U}	1014.05		1030.89	
29	E_{2U}	416.00	398.00	283.90	
30	E_{2U}	416.00		338.17	

VI. References

(1) Schmidt, M. W.; Baldridge, K. K.; Boatz, J. A.; Elbert, S. T.; Gordon, M. S.; Jensen, J. H.; Koseki, S.; Matsunaga, N.; Nguyen, K. A.; Su, S.; Windus, T. L.; Dupuis, M.; Montgomery, J. A. *J. Comput. Chem.* **1993**, *14* (11), 1347–1363.

(2) Piecuch, P.; Włoch, M. *J. Chem. Phys.* **2005**, *123* (22), 224105–224110.
(3) Włoch, M.; Gour, J. R.; Piecuch, P. *J. Phys. Chem. A* **2007**, *111* (44), 11359–11382.
(4) Chai, J.-D.; Head-Gordon, M. *Phys. Chem. Chem. Phys.* **2008**, *10* (44), 6615–6620.
(5) Rappoport, D.; Furche, F. *J. Chem. Phys.* **2010**, *133* (13), 134105–134111.
(6) Billo, E. J. In *Excel for Chemists®*; John Wiley & Sons, Inc., 2011; pp 463–488.
(7) Mozhayskiy, V. A.; Krylov, A. I. *ezSpectrum*.
(8) Eberly, D. http://www.geometrictools.com/ (accessed Jan 29, 2015).
(9) Franck, J.; Dymond, E. G. *Trans. Faraday Soc.* **1926**, *21*, 536–542.
(10) Condon, E. U. *Phys. Rev.* **1926**, *28* (6), 1182–1201.
(11) Chang, J.-L. *J. Mol. Spectrosc.* **2005**, *232* (1), 102–104.
(12) Chang, J.-L. *J. Chem. Phys.* **2008**, *128* (17), 174111–10.
(13) Rodler, M. *J. Mol. Spectrosc.* **1985**, *114* (1), 23–30.
(14) Rodler, M.; Bauder, A. *J. Am. Chem. Soc.* **1984**, *106* (14), 4025–4028.
(15) Koga, Y.; Nakanaga, T.; Sugawara, K.; Watanabe, A.; Sugie, M.; Takeo, H.; Kondo, S.; Matsumura, C. *J. Mol. Spectrosc.* **1991**, *145* (2), 315–322.
(16) Snels, M.; Beil, A.; Hollenstein, H.; Quack, M. *Chem. Phys.* **1997**, *225* (1–3), 107–130.
(17) Åsbrink, L.; Lindholm, E.; Edqvist, O. *Chem. Phys. Lett.* **1970**, *5* (9), 609–612.